ELSEVIER

Journal of Chromatography A, 707 (1995) 87–103

JOURNAL OF CHROMATOGRAPHY A

Free-solution electrophoresis with amplification of small mobility differences by helical flow

Min-Po Shiue[1], Arne J. Pearlstein*

Department of Mechanical and Industrial Engineering, University of Illinois at Urbana–Champaign, 1206 West Green Street, Urbana, IL 61801, USA

Abstract

A description and theoretical analysis is given of a free-solution, three-dimensional electrophoretic field-flow fractionation separation in a concentric circular annulus, in which an axisymmetric swirl flow with velocity components in the axial and azimuthal directions is used to amplify a small difference between the electrophoretic mobilities of two species in a radial electric field. Separation is achieved in the azimuthal direction. The potential of this process is illustrated by calculations (neglecting diffusion) of azimuthal separations of β-lactoglobulins A and B, and racemic denopamine complexed to a stereoselective cyclodextrin. The relative mobility difference for the β-lactoglobulins is about 7%, while that of the denopamine enantiomers (one of which is a potent cardiotonic agent) is about 2%. (Diffusionless) separations of 180° can be achieved with relatively modest angular rotation rates.

1. Introduction

The need for continuous-flow separations of ever higher resolution is driven by a number of factors, including the commercialization of biological macromolecules, natural products, and chiral drugs.

Recently, we have described [1] a new class of continuous field flow fractionation (FFF) separations. These processes, which are based on differential radial migration of two species under the action of a radial force (electrical, centrifugal, etc.) and use of helical flow in a concentric circular annulus (driven by rotation of one cylinder and an applied axial pressure gradient), differ from previous FFF techniques [2] (cf. [3,4] for recent reviews) in several key respects. First, unlike previous FFF processes, these separations do not rely on development of a steady concentration distribution, subsequently subjected to a shear flow that differentially elutes species having different initial distributions in the fluid. Rather, the new class of processes relies on differential advection by the axial and azimuthal components of a helical shear flow to separate species that migrate radially at different rates. Second, as opposed to the usual two-dimensional FFF case in which enrichment and elution occur in the cross-stream and streamwise directions, respectively, the new class of processes is three-dimensional, with force-induced migration, elution, and amplification occurring in the radial, axial, and azimuthal separations, respectively. Third, large separations may be obtainable in relatively small apparatuses, by taking advantage of the long path lengths available to species

* Corresponding author.

[1] Present address: Space and Missiles Center, Los Angeles AFB, El Segundo, CA 90245, USA.

0021-9673/95/$09.50
SSDI 0021-9673(95)00008-9

trajectories that azimuthally wind around the inner cylinder of an annulus.

In this paper, we consider a particular separation process of the class described in Ref. [1], in which two or more species undergo differential electromigration in an applied radial electrical field, and are azimuthally separated by the helical flow. We illustrate the concept by considering, on a diffusionless basis, separation of the enantiomers of denopamine (bound to a stereoselective cyclodextrin), and of β-lactoglobulins A and B. The reader is referred to [1] for a discussions of the more general class of helical flow FFF separations, including more detailed consideration of the diffusion and dispersion processes that may tend to degrade separations of this type.

2. Principle of the separation

We consider the annular space between concentric circular cylinders of radii r_i and r_o, with $r_i/r_o \equiv \eta \leq 1$. The inner cylinder is held fixed, and the outer one rotates at a constant angular velocity $\Omega \mathbf{e}_\theta$. An axial pressure gradient $(dp/dz)\mathbf{e}_z$ drives a net flow through the annulus. Here, $\mathbf{e}_\theta$ and $\mathbf{e}_z$ are unit vectors in the azimuthal and axial directions, respectively.

For a constant-viscosity Newtonian fluid, the velocity field is given by

$$\mathbf{u} = u_\theta(r)\mathbf{e}_\theta + u_z(r)\mathbf{e}_z \tag{1}$$

where the azimuthal and axial components are

$$u_\theta(r) = \frac{\Omega(r - r_i^2/r)}{1 - \eta^2} \tag{2a}$$

$$u_z(r) = \frac{-r_o^2 dp/dz}{4\mu}\left(1 - \frac{r^2}{r_o^2} - \frac{1-\eta^2}{\ln\eta}\cdot\ln\frac{r}{r_o}\right) \tag{2b}$$

respectively, and μ is the absolute viscosity. These profiles are shown in Fig. 1 for $\eta = 0.7$, 0.8, and 0.9. The azimuthal velocity component varies monotonically, and nearly linearly, from zero at the inner (nonrotating) cylinder to a maximum value of Ωr_o at the outer (rotating) cylinder. The variation with the radial coordinate becomes more linear as $\eta \to 1$. The axial velocity profiles are approximately parabolic, becoming increasingly parabolic (and symmetric about $(\eta + 1)/2$) as $\eta \to 1$. The axial velocity attains a maximum at an intermediate radius

$$r^* = \left[\frac{1-\eta^2}{-2\ln\eta}\right]^{1/2} r_o \tag{3}$$

In Eqs. 1 and 2 we have neglected the dependence of viscosity on temperature and composition. Variable viscosity effects will change the quantitative shapes of the velocity profiles (Eqs. 2a and 2b); since, however, as discussed in [1] and below, it is the qualitative features of the axial and azimuthal velocity profiles that are responsible for the separation, we will neglect viscosity variation in this first analysis. We have also neglected secondary flow that might be driven by buoyancy, electro-osmotic, or electrohydrodynamic effects. These effects are discussed in [1] in the context of general helical FFF separations, and in Section 6 below in the specific context of electrophoresis. Finally, we have assumed that this exact solution (1–2) of the Navier–Stokes equations is stable (cf. Joseph [5]), that the flow is fully developed axially, and that end effects are unimportant.

The components are to be separated on the basis of a difference in electrophoretic mobilities, leading to a difference in the rates at which they migrate radially in the annulus under the action of an applied radial electric field. For simplicity, we consider two molecular species in a solvent. Extension to more components is straightforward. The discussion and analysis are substantially the same for nucleic acid fragments, viruses, other supramolecular assemblies, and cells. The present discussion considers deterministic trajectories of molecules of the two species in the absence of diffusion.

The mixture to be separated enters the annulus from a port (e.g., a porous membrane or frit) on the inner cylinder. If a potential difference is established between the two cylinders, then in the resulting radial electric field, the two species will migrate at different rates (depending on their respective mobilities) toward the outer

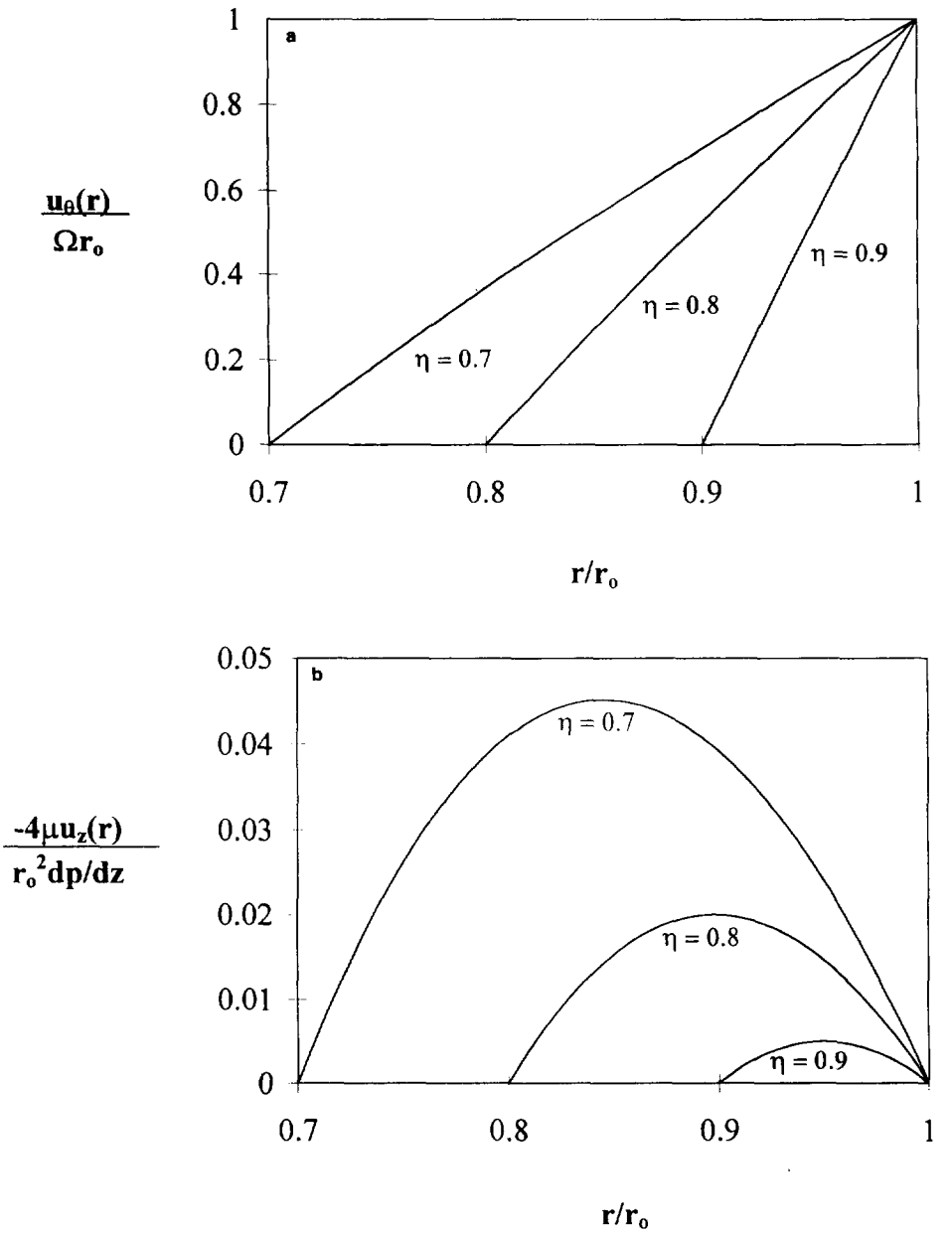

Fig. 1. (a) Radial variation of the dimensionless azimuthal velocity for $\eta = 0.7$, $\eta = 0.8$ and $\eta = 0.9$; (b) radial variation of the dimensionless axial velocity for $\eta = 0.7$, $\eta = 0.8$ and $\eta = 0.9$.

cylinder. In the schematic Fig. 2, we show the trajectory of a single species under the combined effects of the radial electric field and the axial and azimuthal flow.

As discussed in more detail in [1], the axial velocity component decreases monotonically beyond r^*, so that once the slower-migrating species has passed r^*, it has a higher axial velocity than the faster-moving species. Hence, the faster-migrating species spends more time in the part of the flow where the azimuthal velocity component is greatest, and is advanced azimuth-

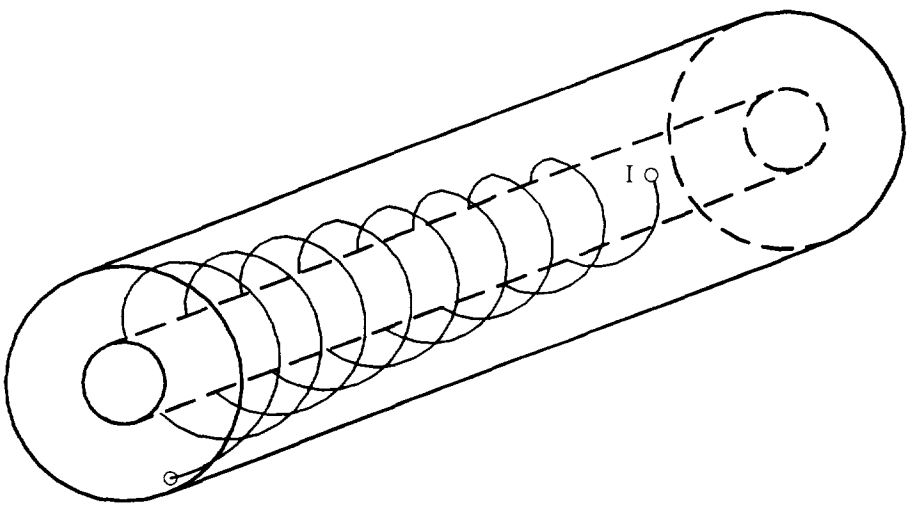

Fig. 2. Schematic illustration of the trajectory of a single species undergoing radial electromigration and axial and azimuthal advection. The label I denotes the injection point on the inner cylinder.

ally relative to the slower-moving species. Thus, the two components emerge (at the exit plane) at different values of the azimuthal coordinate. As shown below, the angular separation can be quite large.

3. Theory

The transport of each species ($k = 1,2$) can be described by a conservation equation

$$\frac{\partial C_k}{\partial t} + \mathbf{u}\cdot\nabla C_k = -\nabla\cdot\mathbf{J}_k \tag{4}$$

where C_k is the concentration of the kth species, u is the fluid velocity, and $\mathbf{J}_k$ is the flux of the kth species. The flux consists of a diffusive contribution and a contribution from electromigration. If the solution is dilute, the flux can be approximated by

$$\mathbf{J}_k = -D_k\nabla C_k - \mu_k C_k\nabla\Phi \tag{5}$$

where μ_k and D_k are the mobility and diffusivity, respectively, of the kth species, and Φ is the potential.

The validity of the transport Eq. 4 is limited by the dilute solution approximations inherent in Eq. 5 (Newman [6]), which is useful for a first analysis. Since the process is continuous, operation with relatively dilute samples is a potentially viable strategy. Given these approximations, the potential is governed by Laplace's equation

$$\nabla^2\Phi = 0 \tag{6}$$

the solution of which is

$$\Phi = \Phi_o + \frac{\Phi_i - \Phi_o}{\ln\eta}\cdot\ln r/r_o \tag{7}$$

Under steady conditions, Eqs. 1, 2, 4, 5 and 7 can be combined to give

$$\frac{u_\theta(r)}{r}\cdot\frac{\partial C_k}{\partial\theta} + u_z(r)\cdot\frac{\partial C_k}{\partial z} - \frac{\mu_k\Delta\Phi}{\ln\eta}\cdot\frac{1}{r}\cdot\frac{\partial C_k}{\partial r} = D_k\cdot\left[\frac{1}{r}\cdot\frac{\partial}{\partial r}\left(r\cdot\frac{\partial C_k}{\partial r}\right) + \frac{1}{r^2}\cdot\frac{\partial^2 C_k}{\partial\theta^2} + \frac{\partial^2 C_k}{\partial z^2}\right] \tag{8}$$

where $\Delta\Phi = \Phi_i - \Phi_o$. We suppose that the mixture to be separated enters the flow through a small opening in the inner cylinder at ($r = r_i$) located near $z = 0$, $\theta = 0$, and that the uniform and steady flux of each species through the opening is given by J_{ko}, so that

$$-D_k \cdot \frac{\partial C_k}{\partial r} - C_k \cdot \frac{\mu_k \Delta \Phi}{r_i \ln \eta} = J_{k0} \tag{9a}$$

We take the remainder of the inner cylinder and the entire outer cylinder to be impermeable to each component, so that

$$-D_k \cdot \frac{\partial C_k}{\partial r} - C_k \cdot \frac{\mu_k \Delta \Phi}{r_i \ln \eta} = 0 \tag{9b}$$

on the remainder of the inner cylinder and

$$-D_k \cdot \frac{\partial C_k}{\partial r} - C_k \cdot \frac{\mu_k \Delta \Phi}{r_0 \ln \eta} = 0 \tag{9c}$$

on the outer cylinder.

We note that the radial coordinate can be scaled with the outer radius or the gap $(r_0 - r_i)$, and that the axial coordinate can be scaled with either of those lengths or the cell length; thus, several nondimensionalizations are possible. We choose one well-suited for analyzing the resolution achievable absent diffusion, constituting an upper bound on the performance of the real system. We scale the radial and axial coordinates as $\rho = r/r_0$ and $y = z/r_0$, respectively, and the concentration as $S_k = D_k C_k / r_0 / J_{k0}$, leading to

$$\alpha \cdot \left(\frac{1 - \eta^2/\rho^2}{1 - \eta^2}\right) \cdot \frac{\partial S_k}{\partial \theta} + \frac{2 \cdot \left(1 - \rho^2 - \frac{1 - \eta^2}{\ln \eta} \cdot \ln \rho\right)}{(1 - \eta^2) \cdot \left(1 + \eta^2 + \frac{1 - \eta^2}{\ln \eta}\right)} \cdot \frac{\partial S_k}{\partial y} - \frac{h_k}{\rho \ln \eta} \cdot \frac{\partial S_k}{\partial \rho} = \frac{1}{Pe_k} \cdot \left[\frac{1}{\rho} \cdot \frac{\partial}{\partial \rho}\left(\rho \cdot \frac{\partial S_k}{\partial \rho}\right) + \frac{1}{\rho^2} \cdot \frac{\partial^2 S_k}{\partial \theta^2} + \frac{\partial^2 S_k}{\partial y^2}\right] \tag{10}$$

where $\alpha = \Omega r_0 / \langle u_z \rangle$ is the dimensionless ratio of the peripheral speed of the outer cylinder to the average speed in the axial direction, $h_k = \mu_k \Delta \Phi / (r_0 \langle u_z \rangle)$ is a dimensionless measure of the field strength, $Pe_k = \langle u_z \rangle r_0 / D_k$ is a Péclet number, and $\langle u_z \rangle$ is the mean axial velocity.

4. Analysis

The goal of the analysis is, then, to compute the dimensionless concentration distributions S_1 and S_2, from which one can determine the best way to collect fractions at the exit plane ($z = L$, $y = \sigma = L/r_0$) according to the composition of the injected sample, the degree of purity desired, and other factors.

Although linear, the partial differential Eq. 10 and its associated boundary conditions constitute a three-dimensional elliptic boundary value problem, for which no simple closed-form solution exists. Moreover, there are two geometric parameters (η and σ) and one fluid mechanical parameter (α), and for each species two other parameters (h_k and Pe_k). Thus, it is useful to analyze the performance of the system in the absence of diffusion, in order to make a preliminary assessment of the effects of η, σ, α and h_k on system performance. We note that in the absence of diffusion, all molecules of a given species that enter the flow at the same point follow the same path in the annulus, leading to the development of two deformed helical trajectories. These trajectories intersect the exit plane (or the outer cylinder, if the dimensionless field strength h is too large) at different points, corresponding to different values of θ and r (dimensionlessly, ρ). The effect of diffusion will be to "smear" these crossing points into closed curves (i.e., contours) of constant concentration in the exit plane. For sufficiently large Péclet numbers (i.e., weak diffusion), the maximum values of the exit plane concentration will nearly coincide with the crossing points for the diffusionless case. This will provide significant guidance in determining favorable values of η, σ, α and h_k in the diffusive computations. (Note that for a given choice of solutes, buffer, pH, etc., h_1 and h_2 are not independent, being proportional to the applied electric field strength.) We note here that for fractionation at the exit plane, the quantities of actual interest are the axial components of the local fluxes, given by $\mathbf{e}_z \cdot \mathbf{N}_k = \mathbf{e}_z \cdot (\mathbf{J}_k - \mathbf{u}C_k)$. However, since the electromigration contribution to $\mathbf{J}_k$ has only a radial component, it contributes nothing to the axial components of $\mathbf{N}_1$ and $\mathbf{N}_2$. The relative magnitudes of the remaining two terms (the Fickian term $D_k \partial C_k / \partial z$ and the axial advection term $u_z C_k$) vary inversely with the Péclet number. Thus, so long as the

Péclet number is not too small (i.e., greater than about 10), the local collection rate will be well-approximated by the product of the axial velocity component and the exit-plane concentration, $u_z C_k$.

As noted above, in the absence of diffusion, the problem reduces to the computation of trajectories of the individual species. In that case, Eq. 10 reduces to a linear hyperbolic partial differential equation (with variable coefficients) which can be integrated exactly. We find that C_k is constant on characteristics given by

$$y_k - y_k^{(i)} = \frac{2 \ln \eta}{h_k \cdot (1-\eta^2) \cdot \left(1+\eta^2+\dfrac{1-\eta^2}{\ln \eta}\right)} \cdot \left[\frac{\rho_k^2}{2} - \frac{\rho_k^4+\eta^4}{4} - \frac{1-\eta^2}{4 \ln \eta} \cdot (2\rho_k^2 \ln \rho_k - \rho_k^2 + \eta^2)\right] \tag{11a}$$

and

$$\theta_k - \theta_k^{(i)} = \frac{\alpha \ln \eta}{h_k(1-\eta^2)} \cdot \left(\frac{\rho_k^2-\eta^2}{2} - \eta^2 \ln \frac{\rho_k}{\eta}\right), \tag{11b}$$

where $y_k^{(i)}$ and $\theta_k^{(i)}$ are the axial and azimuthal coordinates, respectively, at which the species enter the flow at $\rho = \eta$ ($r = r_i$). Eqs. 11a and 11b describe the diffusionless trajectories of the two species.

5. Results

Using the diffusionless analysis developed above, we now illustrate the potential of this method by presenting results for two specific systems. We have considered separation of a protein system (β-lactoglobulins A and B), for which the relative mobility difference is about 7% [7], and the chiral resolution of the enantiomers of denopamine (one of which is a potent cardiotonic agent) complexed with the stereoselective running buffer heptakis(2,6-di-O-methyl)-β-cyclodextrin, for which the relative mobility difference is about 2% [8]. We define a parameter $\gamma = 1 - \mu_2/\mu_1$ as the relative difference in mobilities, and take $\gamma > 0$, so that species 1 is the faster-migrating species. We thus consider h_1 and γ instead of h_1 and h_2.

We are interested in the azimuthal separation achieved at the exit plane. We thus set $y_k - y_k^{(i)} = \sigma$ for each species, use Eq. 11a to compute the corresponding values of ρ_k at the exit plane, and then use Eq. 11b to compute θ_k ($k = 1, 2$) at the exit plane for these values of ρ_k. The difference, $\Delta\theta = \theta_1 - \theta_2$ gives the angular separation at the exit plane. We also remark that there will be some separation in the radial direction at the exit plane, and that there is never any advantage in driving $\Delta\theta$ past 180°.

We begin by noting that, from the fact that α is absent from Eq. 11a and appears linearly in Eq. 11b, one can deduce that the separation is linear in α, so that $\Delta\theta = \Gamma\alpha$, where Γ is a constant that depends on geometry, flow, field strength, and mobility, through the dimensionless parameters h_1, η, γ and σ. Put differently, since each exit value of θ_k (and hence $\Delta\theta$) is proportional to α, one need only compute the constant of proportionality in order to determine the relationship between the flow parameter α and the diffusionless azimuthal separation. We also note that the value of h_1 should be chosen so that the trajectory of the faster-migrating species intersects the exit plane rather than the outer cylinder. This imposes an upper limit on h_1. Also, from the discussion above and in [1], we would like h_1 to be sufficiently large that the faster-migrating species spends some of its residence time near the outer cylinder, where the axial shear is relatively high (so that the faster-migrating species will be held up relative to the slower-migrating species) and the azimuthal velocity is highest (so that the faster-migrating species will be carried around farther in the azimuthal direction than will the slower-migrating one).

Fig. 3a shows $\Gamma = (\Delta\theta)/\alpha$ as a function of h_1 for three different values of η with $\sigma = 5$ and $\gamma = 0.02$ (corresponding to separation of the denopamine enantiomers). For each η there is a vertical asymptote, at which $\Delta\theta$ becomes un-

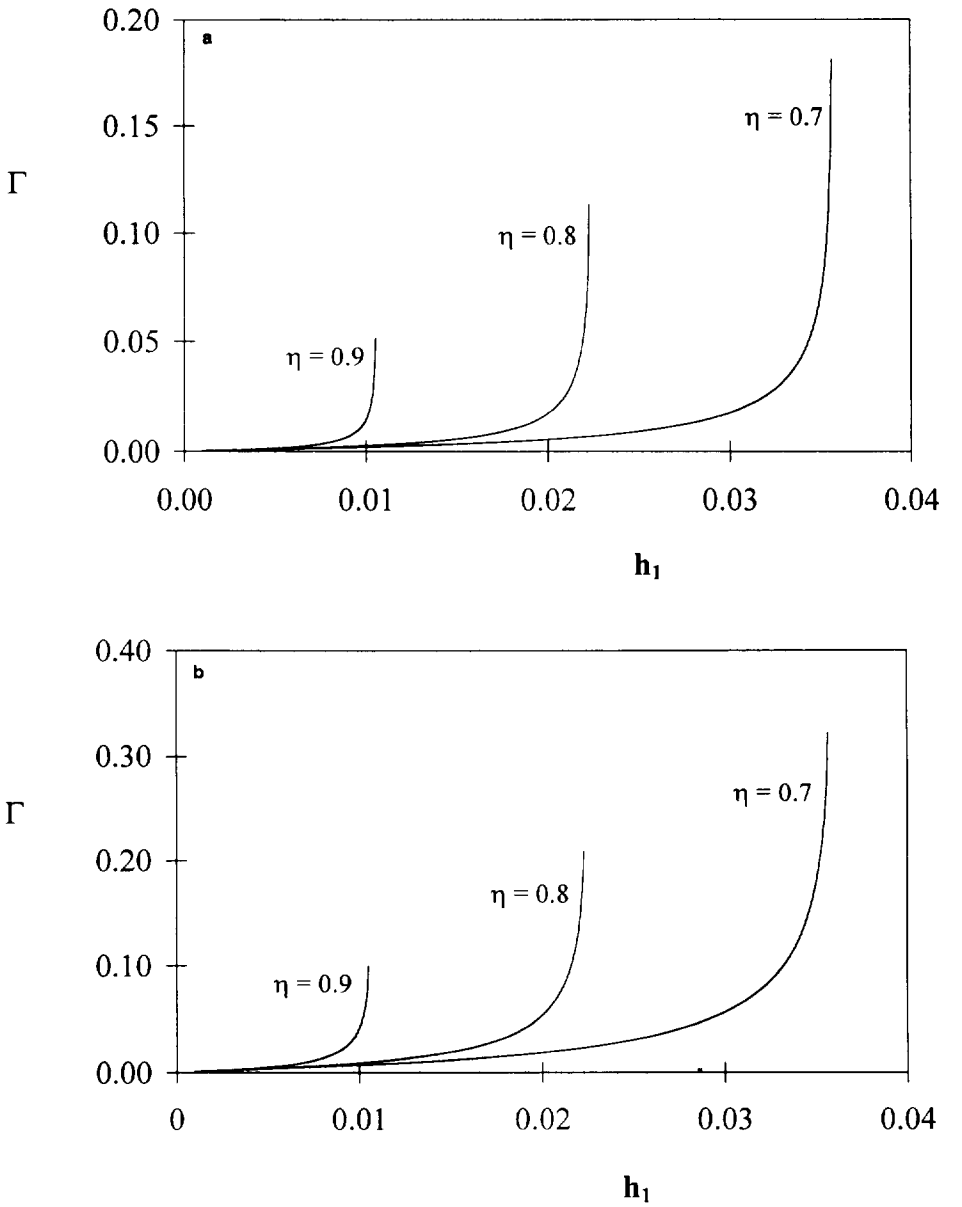

Fig. 3. Variation of $\Gamma = \Delta\theta/\alpha$ with h_1 for $\sigma = 5$, and $\eta = 0.7$, $\eta = 0.8$ and $\eta = 0.9$. (a) $\gamma = 0.02$; (b) $\gamma = 0.07$. The vertical asymptotes correspond to those values of h_1 at which the trajectory of the faster-migrating species intersects the outer cylinder.

bounded for $h_1 = h_1^*$, corresponding to the dimensionless field strength at which, on a diffusionless basis, the trajectory of the faster-migrating species intersects the outer cylinder at the exit plane. For slightly smaller values of h_1, the faster-migrating species comes very close to reaching, and spends a great deal of time near, the outer cylinder, all the while being advected in the azimuthal direction. Meanwhile, the slower-migrating species has not experienced as low an axial velocity, and has been eluted out with a smaller residence time, and less azimuthal advection. It is this effect that is responsible for the very high values of Γ shown as $h_1 \to h_1^*$. We

note that Γ (and hence the azimuthal separation $\Delta\theta$ achievable with a given α) decrease monotonically as h_1 decreases. For sufficiently small h_1, neither species closely approaches the outer cylinder, and there is very little separation. We note that h_1^* increases with decreasing η, since as η decreases, the gap between the cylinders increases and a larger potential drop is required in order for the faster-migrating species to approach the outer cylinder. For a given value of h_1, Γ is a monotonically increasing function of η, indicating that for a given potential drop, better separation is achieved for narrow gaps. This is simply a consequence of the fact that for small gaps ($\eta \approx 1$), the electric field strength varies approximately like $h_1/(1-\eta)$.

Fig. 3b shows similar results for $\gamma = 0.07$. Since we have eliminated the dimensionless parameter h_2 in favor of the relative mobility difference $\gamma = 1 - h_2/h_1$, the vertical asymptotes for each radius ratio η are independent of γ, as each corresponds to the value of h at which the faster-migrating component's trajectory simultaneously intersects the exit plane and the outer cylinder. The degree of separation, as measured by $\Gamma = (\Delta\theta)/\alpha$, is seen to be nearly proportional to γ, at least for the small relative mobility differences considered here.

These results can also be understood in terms of the trajectories of the individual species. For $\sigma = 5$, $\gamma = 0.02$, $\eta = 0.9$, and three successively increasing values of h_1, Fig. 4 shows how the faster-migrating species moves downstream (in the y-direction) as it simultaneously migrates outward towards the outer cylinder. The values of h_1 shown in Fig. 4 correspond to points on the lower part of the Γ–h_1 curve ($h_1 = 0.003$), the rapidly ascending part ($h_1 = 0.009$), and a value $h_1 = 0.0104$ close to the vertical asymptote, respectively. In each case, we see that the trajectory emanates from the inner cylinder at normal incidence, corresponding to the fact that at $\rho = \eta$ the axial velocity (given by Eq. 2b) is zero, while the radial migration rate is non-zero. As the faster-migrating species reaches the radius at which the axial velocity is maximum (see Eq. 3), an inflection point occurs, as shown in Fig. 4b and c. (Note that for the smallest value of h_1 shown, the faster-migrating species reaches the exit plane before reaching r^*.) For the largest value of h_1, Fig. 4c shows that as the faster-migrating species approaches the outer cylinder,

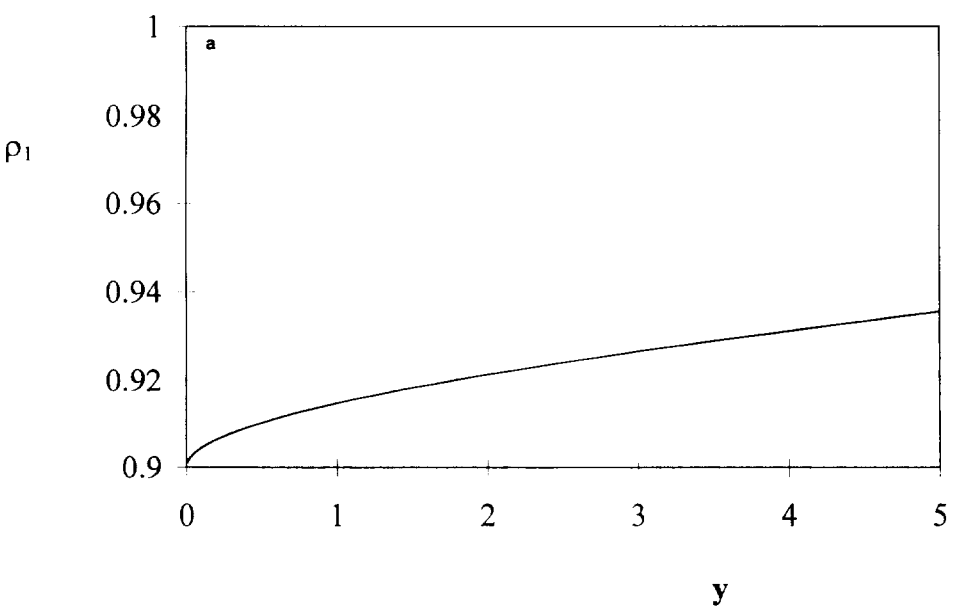

Fig. 4.

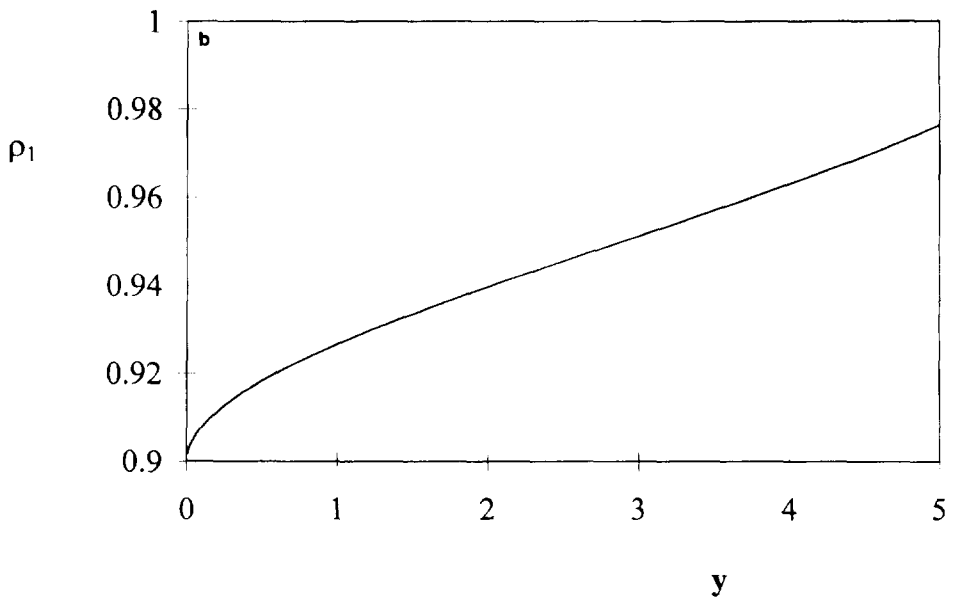

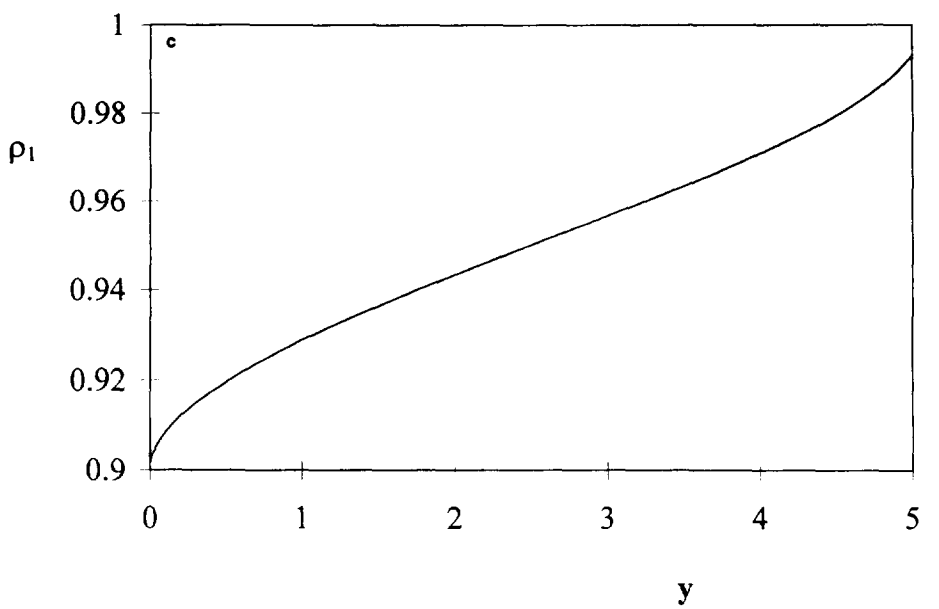

Fig. 4. Axial displacement of the faster-migrating species as it migrates from the inner cylinder towards the outer cylinder for $\eta = 0.9$, $\gamma = 0.02$ and $\sigma = 5$. (a) $h_1 = 0.003$; (b) $h_1 = 0.009$; (c) $h_1 = 0.0104$.

its axial velocity decreases rapidly. It is easy to see that for $h_1 \geq h_1^*$, the trajectory of the faster-migrating species will intersect the outer cylinder at normal incidence. We note that since the dimensionless angular rotation rate α affects neither the axial nor the radial components of the species trajectory (on a diffusionless basis), the results in these figures are independent of α.

In Fig. 5, we examine θ–y projections of the trajectories for $\sigma = 5$, $\gamma = 0.02$, $\eta = 0.9$, and the same values of h_1, with α chosen so that $\Delta\theta = 180°$ at the exit plane. For the smallest value of h_1 shown (Fig. 5a), the faster-migrating species reaches the exit plane before reaching r^* (the radius at which the axial velocity is a maximum). Thus, in this case, the separation does not benefit from the increased residence time of the faster-migrating species (relative to its slower counterpart) in the part of the flow where the angular velocity $u_\theta(r)/r$ is highest. However, as h_1 increases, the value of α required to achieve a 180° separation decreases, as does the total length of the trajectory. Put differently, as h_1 increases, the trajectories corresponding to $\Delta\theta = 180°$ at the exit plane become less tightly wound around the inner cylinder. Since the azimuthal velocity component increases monotonically with radius, we note that the θ–y projections become increasingly steep as y increases.

Finally, for $\sigma = 5$ and $\eta = 0.9$, Figs. 6 and 7 show, for $\gamma = 0.02$ and $\gamma = 0.07$, respectively, how $\Delta\theta = \theta_1 - \theta_2$ varies with axial distance. For $\gamma = 0.02$ and $h_1 = 0.003$, Fig. 6a shows how $\Delta\theta$ varies linearly with α. The largest value of α shown (4100) corresponds to a 180° separation of the two trajectories at the exit plane. As α is successively halved, the exit plane separation is reduced to 90° and 45°. (It is easy to show that the three curves in Fig. 6a can be collapsed to one by dividing the corresponding values of $\Delta\theta$ by α.) More importantly, we see that the curves are not linear in y, and that a large fraction of the separation occurs in the downstream end of the annulus (over 60% of the final $\Delta\theta$ is accomplished in the last one-third of the annulus). This is because the separation between the two species is due to the difference in azimuthal velocity that they experience, and that near the inner cylinder the azimuthal velocity is small (starting at zero at $\rho = \eta$). Thus, it is not until

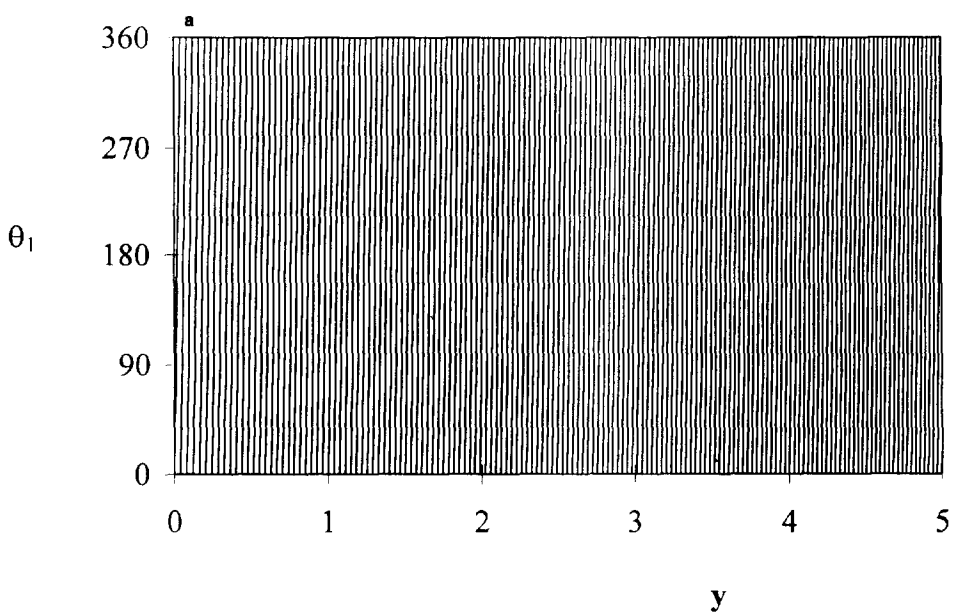

Fig. 5.

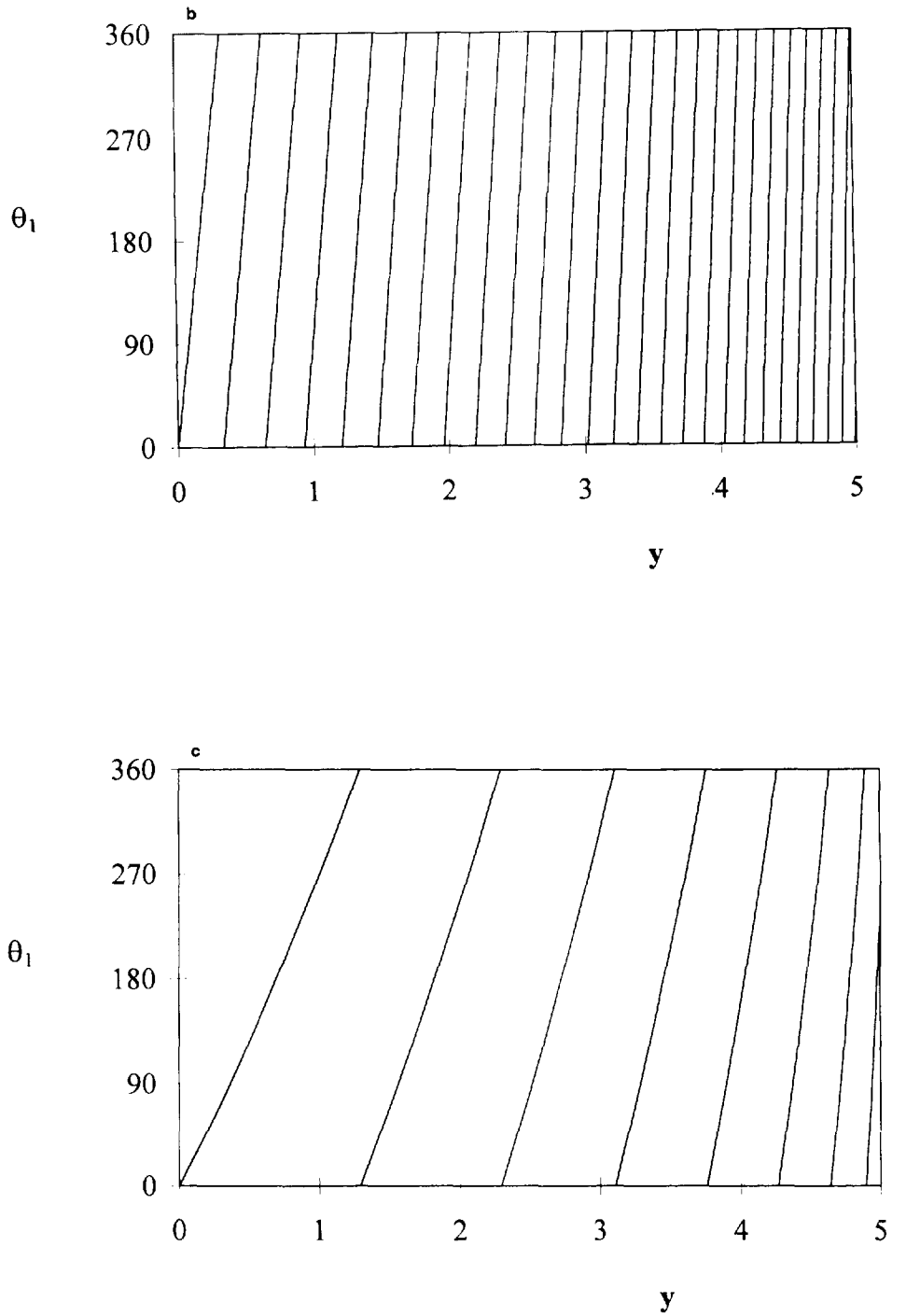

Fig. 5. Azimuthal displacement (in degrees) of the faster-migrating species as it migrates from the inner cylinder towards the outer cylinder for $\eta = 0.9$, $\sigma = 5$ and $\gamma = 0.02$. (a) $h_1 = 0.003$, $\alpha = 4100$; (b) $h_1 = 0.009$, $\alpha = 470$; (c) $h_1 = 0.0104$, $\alpha = 107$. The values of α shown correspond to an azimuthal separation $\Delta\theta = 180°$ between the faster- and slower-migrating components at the exit plane.

the two species have moved out into the flow, where the azimuthal velocity is significant, that a radial separation between faster- and slower-migrating species will be translated into a significant azimuthal separation. Fig. 6b and c show $\Delta\theta$ as a function of the axial coordinate y for $h_1 = 0.009$ and 0.0104, respectively, with the values of α that yield 180° separations at the exit plane h_1. We see that as h_1 increases, the curves become increasingly steep near the exit plane, and an ever larger fraction of the separation is accomplished in the terminal portion of the annulus (over 70% of the separation in the last 10% of the annulus for $h_1 = 0.0104$). This is a direct consequence of the increasingly large retardation of the faster-migration species as its trajectory approaches the outer cylinder. Since its trajectory comes increasingly close to the outer wall as $h_1 \rightarrow h_1^*$, the steepness of the $\Delta\theta$–y curves increases dramatically as the limiting value of h_1 is approached.

If we reconsider Fig. 5c (for $\sigma = 5$, $\eta = 0.9$, $\gamma = 0.02$, $h_1 = 0.0104$ and $\alpha = 107$), in light of these results, we see that by the time the exit plane is reached, the trajectory of the faster-migrating species has wound around the inner cylinder about 2740°. At the exit plane, the slower-migrating species is 180° behind. Thus, we see that a relative mobility difference of 2% has been amplified into a relative azimuthal displacement difference of over 6%.

For $\sigma = 5$ and $\eta = 0.9$, Fig. 7 shows similar plots for $\gamma = 0.07$ and the same values of h_1. The key difference is that the curvature decreases as γ increases, an effect which is not distinguishable at the smallest h_1, but becomes more evident as h_1 increases. Thus, for larger γ, a relatively smaller fraction of the separation is accomplished in the downstream end of the annulus.

We conclude this section with an illustration of the results in dimensional terms. We consider the cyclodextrin-assisted enantiomeric resolution of denopamine discussed above, in a buffer consisting of 25 mM phosphate and 20 mM cyclodextrin, with pH between 2.5 and 3.5 (see Table IV and Fig. 3 of Ref. [8]), for which the relative mobility difference $y = 0.02$ is appropriate. The electrophoretic mobilities of the cyclodextrin-complexed denopamine enantiomers are about $5.9 \cdot 10^{-9}$ m^2 V^{-1} s^{-1} [8]. For the dimensionless results shown in Figs. 4c and 5c, the values of h_1 and α are 0.0104 and 107, respectively. Using the definitions of h_1 and α, we can eliminate the average axial velocity to get $\mu_1 \Delta\Phi/(\Omega r_o^2) = h_1/$

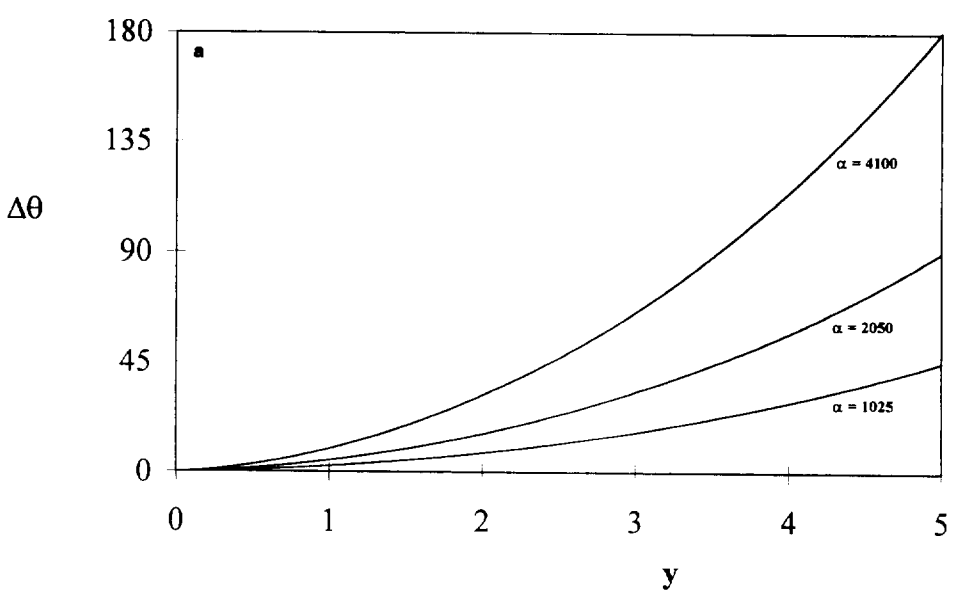

Fig. 6.

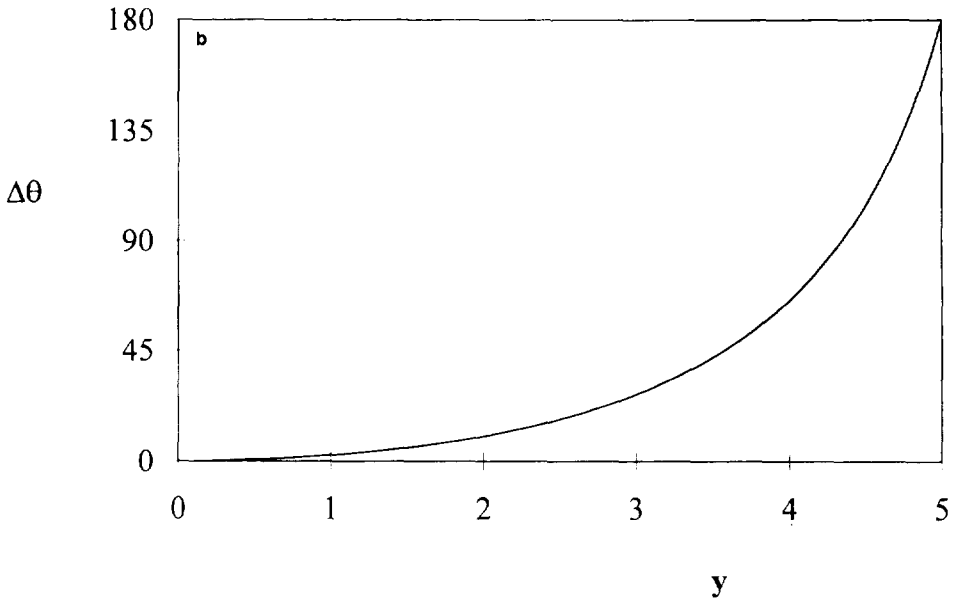

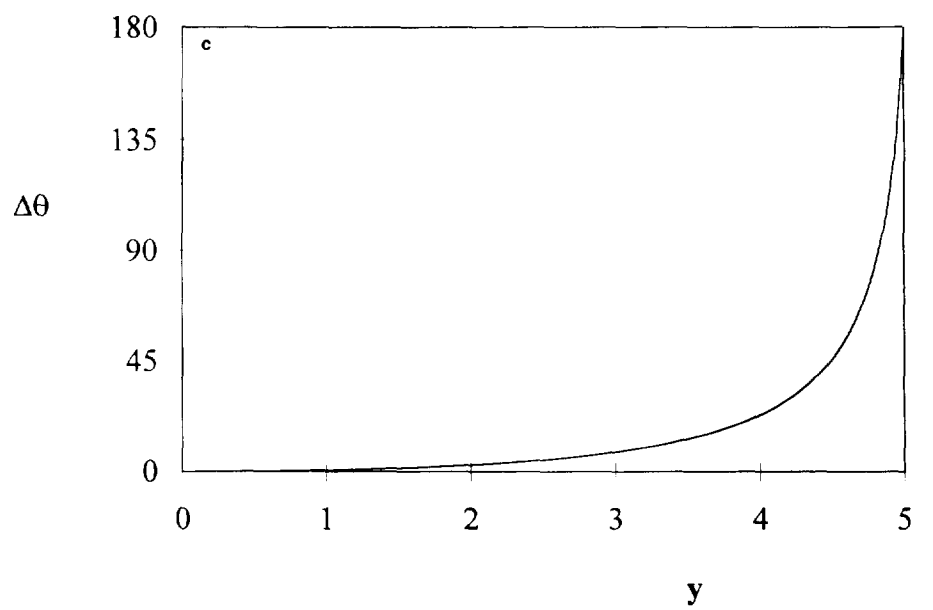

Fig. 6. Axial development of the separation $\Delta\theta$ between the trajectories of the faster- and slower-migrating species for $\eta = 0.9$, $\sigma = 5$ and $\gamma = 0.02$. (a) $h_1 = 0.003$, with three values of α chosen to illustrate the linear dependence of $\Delta\theta$ on α; (b) $h_1 = 0.009$, $\alpha = 470$; (c) $h_1 = 0.0104$, $\alpha = 107$. The values of α shown for (b) and (c) correspond to an azimuthal separation $\Delta\theta = 180°$ between the faster- and slower-migrating components at the exit plane.

$\alpha = 9.7 \cdot 10^{-5}$, from which it follows that a (diffusionless) separation of the type shown in Figs. 4c and 5c can be achieved for combinations of the rotation rate, outer radius, and potential difference satisfying $\Omega r_o^2/\Delta\Phi = 6.0 \cdot 10^{-5}$ m^2 V^{-1} s^{-1}. We thus see that the choice $\Omega = 5$ rpm and $r_o = 5$ cm gives $\Delta\Phi \approx 22$ V, a relatively modest potential difference across a 0.5 cm annular gap (for $\eta = 0.9$), and one quite comparable to the 20 V difference employed by Scott [9] across a 2.5 cm gap in a very different annular electrophoresis system. [For these conditions, the average axial fluid velocity is found to be about 0.025 cm/sec, corresponding to a mean residence time of about 17 min for a cell with $\sigma = 5$ ($L = 25$ cm)].

6. Effects of secondary flow and diffusion

The results presented above were obtained under the assumptions that the velocity field in Eq. 4 corresponds to the helical flow in Eqs. 2a and 2b, and that the diffusive terms on the right-hand side of Eq. 10 are negligible.

Deviations from the flow predicted by Eqs. 2a and 2b are customarily referred to as "secondary flow", and would generally be thought to degrade the separation by indiscriminately changing the trajectories of fluid elements in which one species was enriched relative to the other. In extreme cases, the secondary flow can be turbulent, greatly accelerating molecular mixing among fluid elements.

The flow may depart from Eqs. 1 and 2 for several reasons. First, Eqs. 1 and 2 may be unstable. Specifically, the Navier–Stokes equations, of which Eqs. 1 and 2 are a solution, constitute a non-linear system of partial differential equations, and can have more than one long-time solution for a given combination of Ω and dp/dz. The stability properties of Eqs. 1 and 2 are reasonably well understood [5], and it is known that for sufficiently small values of dp/dz, Eqs. 1 and 2 are stable. For the range of flowrates likely to be of interest in this separation, stability of Eqs. 1 and 2 is unlikely to be an issue. Second, sample introduction at a port on the inner cylinder necessarily leads to some deviation from Eqs. 1 and 2. For a well-designed port, the effects on the flow will be highly localized. Since the two species are unseparated

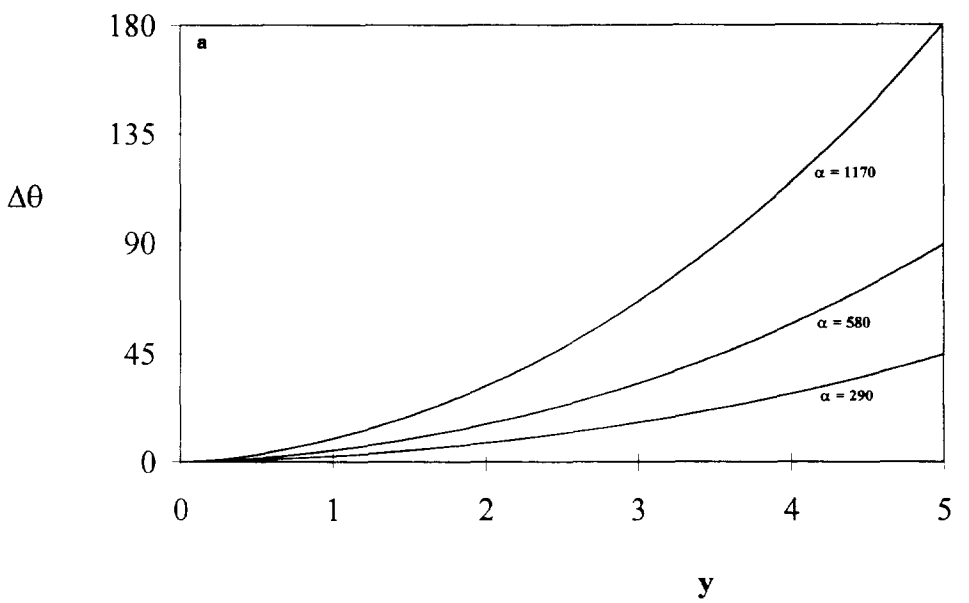

Fig. 7.

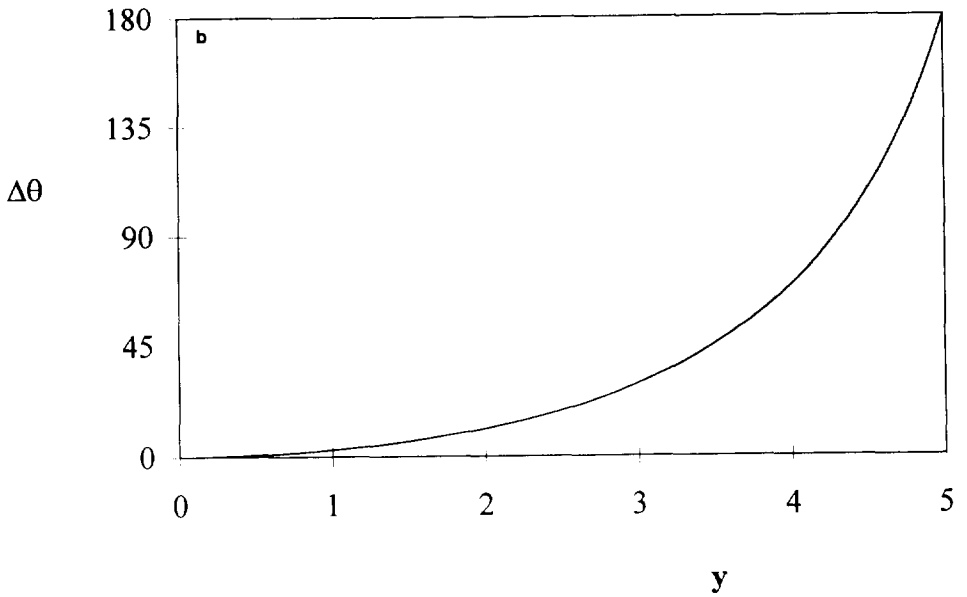

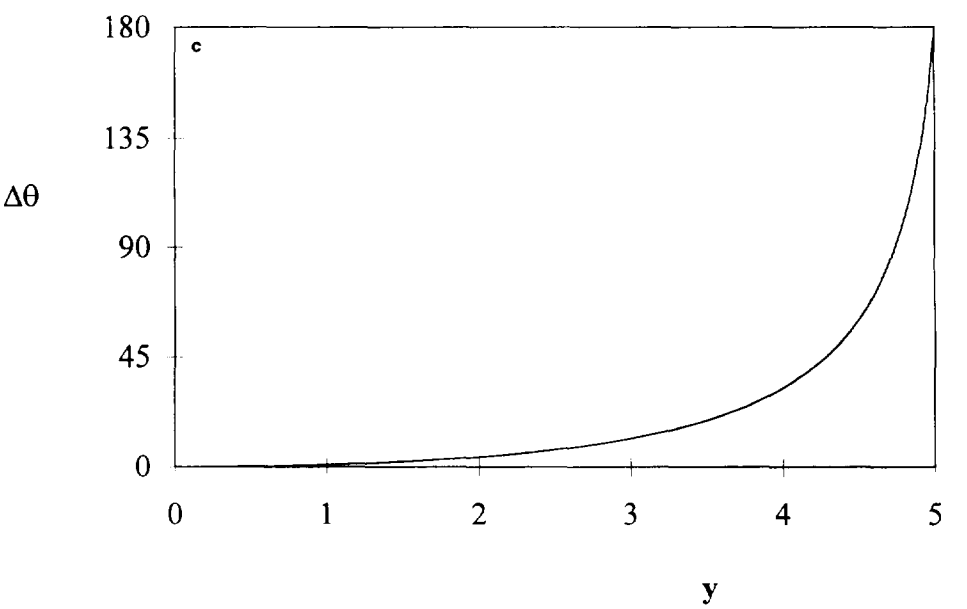

Fig. 7. Axial development of the separation $\Delta\theta$ between the trajectories of the faster- and slower-migrating species for $\eta = 0.9$, $\sigma = 5$ and $\gamma = 0.07$. (a) $h_1 = 0.003$, with three values of α chosen to illustrate the linear dependence of $\Delta\theta$ on α; (b) $h_1 = 0.009$, $\alpha = 147$; (c) $h_1 = 0.0104$, $\alpha = 45$. The values of α shown for (b) and (c) correspond to an azimuthal separation $\Delta\theta = 180°$ between the faster- and slower-migrating components at the exit plane.

at the point of introduction, and since most of the separation occurs at radii in excess of r^* and downstream of the sample port, the local effects on the flow should not seriously degrade the separation. Third, deviations from Eqs. 1 and 2 may occur due to forces not accounted for in the momentum balance leading to Eqs. 1 and 2. Among these are buoyancy [10,11], electroosmotic, and electrohydrodynamic forces.

Gravitationally driven convection necessarily arises whenever $\nabla\rho \times \mathbf{g} \neq \mathbf{0}$ [12]. Application of a potential difference across a conducting fluid leads to passage of a current, which leads to the generation of heat, and hence temperature variations within the annulus. The temperature gradient will have a significant radial component, as well as axial and azimuthal components, the latter two associated with spatial variation of electrical conductivity due to nonuniform solute distribution. Since the density depends on temperature, we will have a density gradient with at least a radial component. Since there is no alignment of the cell for which $\mathbf{e}_r$ is everywhere parallel to $\mathbf{g}$, gravitationally driven convection must occur if the separation is conducted at a non-zero gravitational acceleration. In addition, density variations arise from non-uniform solute distribution (an inevitable consequence of any separation).

There are several means by which gravitationally driven convection can be minimized. First, gravitationally driven convection can be largely eliminated by conducting the process in the microgravity environment of space. Short of going to a microgravity environment, the effects of gravitationally driven convection can be minimized in other ways. One of the more attractive methods over the years has been rotation. Kolin [13–15] and Hjertén [16] have used electromagnetically driven and rigid-body rotation, respectively, to achieve considerable inhibition of buoyancy-driven convection in continuous-flow, free-solution electrophoresis. Kolin attributed the reduction in convective motion to continual reorientation of the density gradient with respect to the gravitational field, leading to continuous changes in the direction of the gravitationally-driven flow at any point. Due to viscous effects, these relatively high-frequency motions are necessarily much weaker than the gravitationally driven flow that would arise in the absence of continuous reorientation. There is good reason to believe that the shear-driven rotation in the present flow will have similar effects. Finally, we note that one can increase the importance of rotational reorientation by rotating the inner and outer cylinders at angular velocities $\Omega_{rgd}\mathbf{e}_\theta$ and $(\Omega + \Omega_{rgd})\mathbf{e}_\theta$, respectively. This has the effect of adding a rigid body rotation to the flow, without altering the helical shear responsible for the separation.

However, buoyancy-driven motion associated with the centrifugal acceleration (due to rotation) is not inhibited by reducing the gravitational acceleration. Fortunately, for the rotation rates likely to be of interest, this effect, while not zero, will probably be small. (In the dimensional example considered at the end of the previous section, the magnitude of the centrifugal acceleration is about 0.013% that of the normal gravitational acceleration.)

Additional types of secondary flow, which are overshadowed by buoyant convection in many electrophoretic separations at normal gravity, can become important in the absence of significant buoyancy-driven convection. Specifically, electrohydrodynamic and electroosmotic effects have plagued several previous attempted electrophoretic separations in a microgravity environment. The corresponding body force is the product of the local charge density and the electric field strength [6]. As distinct from most continuous-flow electrophoresis experiments in which the flow and field are not orthogonal, the present separation minimizes electrohydrodynamic effects by ensuring that the driving force (i.e., the electric field) is nominally radial. Since the nominal velocity field (Eqs. 1 and 2) has no radial component, the primary contribution of the electrohydrodynamic force can be absorbed in the radial component of the pressure gradient in the radial momentum balance, as discussed by Newman [6]. Secondary contributions, due to spatial variation of the electrical conductivity, will be smaller in the present configuration than in traditional electrophoresis cells

[17,18] due to the imposed helical flow. These forces can be further reduced by reducing the sample concentration, a strategy which is less unattractive in the present continuous process than in batch processes.

The effects of diffusion on the present separation may be significant, as discussed in [1] for the general class of helical flow FFF separations. There, we show that in addition to the direct effects of diffusion evident in the three terms on the right-hand side of Eq. 10, one must also consider the effects of diffusion-driven dispersion, wherein diffusion of molecules into or out of fluid elements with different velocities can lead to significant departures from the (diffusionless) trajectories computed herein. A quantitative discussion of the extent to which diffusion will degrade this electrophoretic separation awaits a full analysis of Eq. 10 and the associated boundary conditions.

7. Conclusions

Use of helical flow to amplify small electrophoretic mobility differences in order to achieve large separations in a relatively small geometry, with separation accomplished in the azimuthal direction, is shown to be potentially attractive. The actual performance of the technique will depend on the importance of diffusion and dispersion, as well as on the importance of secondary flows superimposed upon the nominal helical flow regime.

Acknowledgements

The authors are grateful to Professor V.L. Vilker for helpful discussions, and to Professor Vilker and Dr. K.D. Cole for providing mobility data for the β-lactoglobulin system.

References

[1] A.J. Pearlstein and M.-P. Shiue, Sep. Sci. Tech., in press.
[2] J.C. Giddings, Sep. Sci. Tech., 1 (1966) 123.
[3] L.F. Kesner and J.C. Giddings, in P.R. Brown and R.A. Hartwick (Editors), High Performance Liquid Chromatography, Wiley, New York, 1991.
[4] J.C. Giddings, Unified Separation Science, Wiley, New York, 1991.
[5] D.D. Joseph, The Stability of Fluid Motions I, Springer, Berlin, 1976, Ch. 6.
[6] J. Newman, Electrochemical Systems, Prentice-Hall, Englewood Cliffs, NJ, 1973.
[7] K.D. Cole, P.W. Todd, K. Srinivasan and B.K. Dutta, J. Chromatogr. A, in press.
[8] H. Nishi, Y. Kokusenya, T. Miyamoto and T. Sato, J. Chromatogr. A, 659 (1994) 449.
[9] C.D. Scott, Sep. Sci. Tech., 21 (1986) 905.
[10] D.A. Saville, in M.J. Rycroft (Editor), Space Research XIX, Pergamon, Oxford, 1979.
[11] D.A. Saville, PhysicoChemical Hydrodyn., 1 (1980) 297.
[12] A.J. Pearlstein, J. Phys. Chem., 89 (1985) 1054.
[13] A. Kolin, Proc. Natl. Acad. Sci. U.S.A., 46 (1960) 509.
[14] A. Kolin, J. Chromatogr., 26 (1967) 164.
[15] A. Kolin, J. Chromatogr., 26 (1967) 180.
[16] S. Hjertén, Ark. Kemi, 13 (1958) 151.
[17] M.J. Clifton, Electrophoresis, 14 (1993) 1284.
[18] H. Roux-Debalmann, C. Burgand and V. Sanchez, Sep. Sci. Tech., 26 (1991) 1481.